THE JOURNAL OF PHYSICAL CHEMISTRY A

Article

Cite This: J. Phys. Chem. A 2019, 123, 10772−10781

pubs.acs.org/JPCA

Molecular Dynamics of Combustion Reactions in Supercritical Carbon Dioxide. 6. Computational Kinetics of Reactions between Hydrogen Atom and Oxygen Molecule H + O_2 ⇌ HO + O and H + O_2 ⇌ HO_2

Chun-Hung Wang,[†] Artëm E. Masunov,*[,†,‡,§,∥,⊥] Timothy C. Allison,[#] Sungho Chang,[¶] Chansun Lim,[▽] Yuin Jin,[▽] and Subith S. Vasu*[,○]

[†]NanoScience Technology Center, University of Central Florida, 12424 Research Parkway, Orlando, Florida 32826, United States

[‡]School of Modeling, Simulation, and Training, University of Central Florida, 3100 Technology Parkway, Orlando, Florida 32816, United States

[§]Department of Chemistry, University of Central Florida, 4111 Libra Drive, Orlando, Florida 32816, United States

[∥]South Ural State University, Lenin pr. 76, Chelyabinsk 454080, Russia

[⊥]National Research Nuclear University MEPhI, Kashirskoye shosse 31, Moscow 115409, Russia

[#]Southwest Research Institute, San Antonio, Texas 78238, United States

[¶]KEPCO Research Institute, Daejeon 34050, Korea

[▽]Hanwha Power Systems, Seongnam, Gyeonggi 13488, Korea

[○]Center for Advanced Turbomachinery and Energy Research (CATER), Mechanical and Aerospace Engineering, University of Central Florida, Orlando, Florida 32816, United States

Supporting Information

ABSTRACT: Reactions of the hydrogen atom and the oxygen molecule are among the most important ones in the hydrogen and hydrocarbon oxidation mechanisms, including combustion in a supercritical CO_2 (sCO_2) environment, known as oxy-combustion or the Allam cycle. Development of these energy technologies requires understanding of chemical kinetics of H + O_2 ⇌ HO + O and H + O_2 ⇌ HO_2 in high pressures and concentrations of CO_2. Here, we combine quantum treatment of the reaction system by the transition state theory with classical molecular dynamics simulation and the multistate empirical valence bonding method to treat environmental effects. Potential of mean force in the sCO_2 solvent at various temperatures 1000−2000 K and pressures 100−400 atm was obtained. The reaction rate for H + O_2 ⇌ HO + O was found to be pressure-independent and described by the extended Arrhenius equation 4.23×10^{-7} $T^{-0.73}$ exp(−21 855.2 cal/mol/RT) cm^3/molecule/s, while the reaction rate H + O_2 ⇌ HO_2 is pressure-dependent and can be expressed as 5.22×10^{-2} $T^{-2.86}$ exp(−7247.4 cal/mol/RT) cm^3/molecule/s at 300 atm.

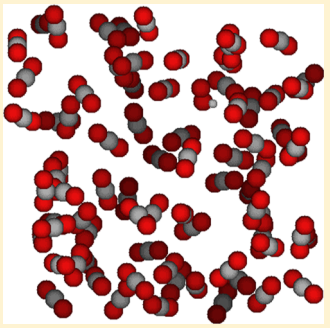

1. INTRODUCTION

The chain-branching and chain-terminating chemical reactions between atomic hydrogen and molecular oxygen are among the most significant combustion reactions[1]

$$H + O_2 \rightarrow HO + O \quad (R1)$$

$$HO + O \rightarrow H + O_2 \quad (R1r)$$

$$H + O_2 \rightarrow HO_2 \quad (R2)$$

$$HO_2 \rightarrow H + O_2 \quad (R2r)$$

$$HO_2 \rightarrow HO + O \quad (R3)$$

$$HO + O \rightarrow HO_2 \quad (R3r)$$

These reactions are the critical part of all the hydrogen and hydrocarbon oxidation mechanisms. Characteristics of hydrogen and hydrocarbon combustion processes, such as flame speeds and ignition delay times are controlled by chain-branching R1 and chain-terminating R2. The understanding of chemical kinetics of these reactions is important in many engineering tasks, such as engine development. Because many combustion reactions are pressure-dependent, the collisional energy transfer of the surrounding mixture (bath gas) influences rate constant *k*. Recently, combustion in supercritical CO_2 environment replacing air (Allam cycle) was

Received: September 16, 2019
Revised: October 22, 2019
Published: December 10, 2019

DOI: 10.1021/acs.jpca.9b08789
J. Phys. Chem. A 2019, 123, 10772−10781

proposed[2,3] to increase the power conversion efficiency and to reduce the generation of greenhouse gases. As a part of our efforts to further develop this technology, we have modeled equation-of-state parameters,[4] developed reduced combustion mechanism,[5] and performed counterflow diffusion flame analyses[6] in sCO_2 environment. We also developed the force field to describe water and carbon dioxide in a mixture supercritical state,[7] investigated potential energy surfaces (PESs) of reactions with the existence of CO_2 by density-functional theory (DFT) calculation,[8−11] and predicted the rate constant k of several important combustion reactions in high pressure of CO_2 by molecular dynamics (MD)[12−15] and DFT simulations.[16,17] In this contribution, we report advances in computational methods of reaction rate prediction in supercritical CO_2 and apply these methods to study R1 and R2.

The rates of R1 and R2 in the gas phase have been studied experimentally and theoretically since 1960s. Recent experiments on endothermic R1 reaction by a shock tube using tunable diode laser absorption of H_2O near 2.5 μm to monitor OH concentration had been performed by Hong et al.[18] at 1100−1530 K and 2 atm. The results were similar to Masten et al.,[19] Hwang et al.,[20] and Yu et al.[21] measured rate constant by shock tube via OH absorption at 950−3100 K, and the difference between these two groups was reported in O_2 vibrational relaxation. Laser flash absorption was performed by Du and Hessler at 2000−5300 K,[22] and the results showed the relaxation effect does not influence the rate constant. Yuan et al. applied shock tube, laser absorption, and modeling techniques to evaluate the rate constant at 1050−2700 K.[23] Shin and Michael used a laser photolysis-shock tube technique to measure the rate constant at 1103−2055 K.[24] Other earlier studies were performed by flash photolysis and/or the shock tube technique.[25−27]

Exothermic and temperature-independent R2 is a chain-terminating reaction of importance for hydrogen and hydrocarbon combustion as one of the primary channels in the release of energy and the consumption of O_2. The R2 rate constant was studied in a low-pressure limit[20,28−31] by shock tube experiments, low-pressure limit[32,33] and high-pressure[27,33] limit by laser flash photolysis and a flow reactor experiment.[34] Reactions of the high-pressure limit in a supercritical water environment was studied by Janik et al. using pulse radiolysis to understand water-cooled nuclear reactor chemistry.[35] The results showed a 4-fold increase of the rate constant from room temperature to 350 °C. Based upon our previous supercritical CO_2 study,[12−15] gas-phase free energy is strongly perturbed by the environment. However, the rate constant of bimolecular R1 with more than one product is consistent with the gas-phase high-pressure limit because collisional repopulation of states depleted by the reaction is fast enough to maintain thermal equilibrium distribution of states.[36]

PES of a hydroperoxyl radical has been evaluated theoretically because accurate PES is the key for further studies. Combined-hyperbolic-inverse-power-representation (CHIPR),[37,38] Xu−Xie−Zhang−Lin−Guo (XXZLG),[39−41] diatomics-in-molecules (DIM),[42−44] reproducing kernel Hilbert space,[45] double many-body expansion (DMBE) IV,[46,47] Melius−Blint (MB),[48] and ab initio theory determined[49−55] PESs have been proposed to explore bound vibrational states. R1 reaction has been studied in several groups since 1960s. For example, Teixidor and Varandas performed quantum scattering calculation by applying CHIPR to consider J-dependence and calculate the rate constant of R1.[56,57] Lin et al.,[58] Teitelbaum et al.,[59] Leforestier and Miller,[60] and Viel et al.[61] used a quantum wave packet-based statistical model and semiempirically corrected ab initio calculated DMBE IV PES to calculate the rate constants of R1 and R1r. Pradhan et al. reported DIM PES with improved long-distance behavior to calculate the rate constant of R1r.[62] Statistical adiabatic channel model/classical trajectory calculation was performed between 0 and 5000 K by Harding et al.[63] and allowed to account for angular momentum conservation. Troe and Ushakov developed TU PES and presented classical trajectory calculation of rate constants of R1r and R2r between 300 and 5000 K.[64] A coupled-state, statistical capture model using CASSCF was performed by Kłoz et al. to study reaction dynamics and evaluate k of R1 and R1r.[65] Rate constants between 250 and 5500 K by variational transition state theory (VTST)[66] with the Rice−Ramsperger−Kassel−Marcus (RRKM) statistical model were obtained by Millar and Garrett.[67] Reaction path-based VTST using MB PES was also applied by Rai and Truhlar between 200 and 2500 K that is based upon a rigid rotor and an independent normal mode.[68] Yang and Klippenstein introduced variable reaction coordinate TST (VRC-TST) using DMBE IV PES to further consider angular momentum conservation and rotational/bending couplings and anharmonicities.[69] The results presented that the rate constant of R1 is independent of temperature. Germann and Miller applied flux−flux autocorrelation function methods which are similar to TST to calculate R1r and R2r rate constants as high as 10 000 atm as a function of collision frequency.[70] Rate constants of R1 and R1r were studied by a quasiclassical trajectory method along with XXZLG,[71,72] DMBE IV,[73,74] MB,[74,75] or other updated ab initio[76,77] PES between 150 and 3000 K. Comparisons of the accuracy of PES between various methods were also performed.[78,79]

The deep (∼55 kcal/mol) well on the potential energy surface corresponds to the addition of a hydrogen atom to an oxygen molecule (reaction R2)[80] and indicates the existence of a highly reactive HOO intermediate. High density of states in this deep well makes it difficult to predict the rate constant k_{R2} accurately. VRC-TST combined with multireference configuration interaction by Harding et al.[81,82] or CASPT2/aug-cc-pVTZ by Sellevåg et al.[83] was applied to calculate the rate constant in the high-pressure limit. Studies of the rate constant pressure-dependence by the RRKM theory were performed by Bates et al.,[30] Himmer and Roduner,[84] Duchovic et al.,[85] and Dobbyn et al.[86] Troe and Ushakov applied quantum capture, adiabatic channel, and classical trajectories to evaluate the rate constant in a broad temperature range (0−5000 K).[87] Recently, pressure-dependence of k_{R2} was also predicted taking into account different collision efficiencies in multicomponent bath gas.[88] Lin et al. used improved XXZLG[89] and DMBE IV[58] PES to calculate the rate constant of R2. In addition, k of R2 was also calculated based upon DMBE IV PES by various research groups[59,84,90−92] and upon simplified statistical adiabatic channel model by Troe.[93,94] Zuo et al. concluded the computational methods developed so far and discussed the pros and cons between these methods.[95]

Despite numerous experimental and computational studies of the title reactive system, none of them investigated kinetics in high-pressure (supercritical) CO_2 environment. In this contribution, we aim to predict the rates at 100−400 atm of CO_2. Our methodology was inspired by Akiya and Savage work, who studied hydrogen peroxide dissociation (H_2O_2 →

DOI: 10.1021/acs.jpca.9b08789
J. Phys. Chem. A 2019, 123, 10772−10781

2HO) in supercritical H_2O environment.[96] They combined quantum mechanical and classical MDs methods to describe the reactive system and supercritical H_2O environment, respectively. The reaction constant k was derived from the general form of the Eyring–Polanyi equation based upon TST[97]

$$k = \kappa\left(\frac{k_B T}{h}\right)\exp\left(-\frac{\Delta G^{\ddagger}}{RT}\right) \quad (1)$$

where κ is the transmission coefficient, k_B is Boltzmann constant, and $\Delta G^{\ddagger}$ is the free energy of activation. The equation is applied in the study of gas and condensed phase without relevance of the collision model. While κ was set to be unity to neglect back scattering effects, $\Delta G^{\ddagger}$ was determined by the free energy difference between the transition state and reactants in gas phase ΔG_{gas}, calculated by means of quantum mechanics. In supercritical environment, solvation free energy difference ΔG_{sol} between the transition state and reactants will also contribute to $\Delta G^{\ddagger}$. In this work, we extended their approach and evaluated free energy along the entire range of the reaction coordinate r using potential of mean force (PMF) $\Delta G^{\ddagger}$

$$\Delta G^{\ddagger}(r) = \Delta G_{gas}(r) + \Delta G_{sol}(r) \quad (2)$$

where $\Delta G_{gas}(r)$ is gas-phase activation energy and $\Delta G_{sol}(r)$ is the change of Helmholtz free energy in the presence of solvent.

In order to produce PMF, we employed classical MD with a multistate empirical valence bond (MS-EVB) method.[98,99] Variable number of explicit CO_2 molecules were included in MD simulations to tune the density of the fluid. To describe bond breaking in the reactive system with empirical force field, we used the MS-EVB method, which is able to reproduce reactive PES and bridge the gap between quantum and classical mechanics. The PMF at various temperatures and densities of CO_2 was determined by umbrella sampling (US),[100] with CO_2 solvent molecules equilibrated and the reaction coordinate constrained in a stepwise manner. A series of windows along with the reaction coordinate were determined a priori to perform classical MD simulation and then combined by the weighted histogram analysis method (WHAM).[101] To the best of our knowledge, this work represents the first theoretical investigation of the rate constants of R1, R2, and R2r in the supercritical CO_2 environment.

2. COMPUTATIONAL DETAILS

2.1. Ab Initio Calculations. The high-level ab initio method CCSD[102−104] with Dunning's correlation consistent basis set cc-pVDZ[105] was selected for geometry optimization and vibrational analysis of HO_2, O_2, and OH (C_s, $D_{\infty h}$, and $C_{\infty v}$ symmetry, respectively) in the gas phase. Single point calculations at CCSD(T)/aug-cc-pVQZ[106] theory level were performed to obtain more accurate energies. Transition state TS1 was located by a gradient minimization technique (keyword Opt = TS). Transition state TS2 was determined by canonical variational TST[36,107] because the reaction R3 has no well-defined TS. Several nonstationary structures were optimized while keeping the O−O bond length constrained. The structure with the highest Gibbs free energy along the reaction path (approximated by O−O bond) was taken to be the generalized TS2. In addition, empirical corrections to TS energies were applied to match the experimentally observed reaction rates, as described in Section 2.3 to fit the pressure-dependent results from the AramcoMech 2.0 database.[18] All the quantum chemical calculations were performed with the Gaussian16 program.[108]

2.2. Rate Constant Calculations. The reaction process considered here begins with collision of the initial reactants, forming a HO_2 intermediate over low activation barrier TS1 (entrance channel). Vibrationally excited HO_2 may then recross TS1 back to the reactants (reaction R2r), dissociate to the products via TS2 (reaction R1), or get stabilized by collisions with the bath gas (reaction R2). Density of states and high-pressure limiting rate coefficients for the entrance channel were calculated using TSTRATE, a modified version of the UNIMOL program,[109] included in a GPOP program suite.[110] Tunneling effects were taken into account using implementation of the asymmetric Eckart potential.[111] The SSUMES[112] program suite was used to solve the steady-state unimolecular master equations based upon the RRKM theory.[113] A single molecule HO_2 is dissociated into the products HO and O, or back into reactants H and O_2. Unimolecular reactions occur at a certain nonzero rate only if the reacting molecules possess an internal energy exceeding the activation energy. In addition, active molecules are deactivated or produced by inelastic collision with the heat bath molecules. In this study, the CO_2 was selected as buffer gas. The energy grain size used was set to a default value of 100 cm^{-1}, which typically gives converged results for combustion reactions.[114] Collisional energy transfer probability was estimated using an exponential-down model,[115] and collision frequency was estimated by assuming the Lennard-Jones (LJ) potential. The LJ parameters of HO_2 were taken to be σ = 4.196 Å and ε/k_B = 289.3 K.[116] The pressure-dependent rate constants were calculated by solving the energy grained, multiple-well master equation and produced the branching fractions for HO_2 dissociation into the products (reaction R1) and stabilization (reaction R2). The truncation threshold was set to 50 energy grains. Moderate variations (5−100) in this truncation threshold did not have a sizable effect on the outcome. In the end, calculated rate constants were fitted by least square regression into the extended Arrhenius equation

$$k = AT^{n}\exp\left(-\frac{E_a}{RT}\right) \quad (3)$$

where A is preexponential factor, n is empirical constant, and E_a is phenomenological activation energy.

2.3. MDs Simulations. Classical MD simulations were performed in CHARMM version c42b1,[117,118] and PES was investigated by relaxed scan of the bond lengths from 0.5 to 4.5 Å. The force field parameters for HO_2, HO, O_2, H, and O were initially estimated by CHARMM General Force Field (CGenFF) program[119] to match the experimental bond lengths and vibrational frequency experimental values taken from NIST database.[120] Then, (i) force constants for bond stretching and angle bending and (ii) σ and ε of the atoms in HO_2 were fine-tuned to reproduce the accurate PESs of HO_2 dissociations in MS-EVB approximation (see Appendix 1 in Supporting Information for more details). To insure the accurate transcritical behavior, the force field parameters for CO_2 molecules were adopted from TraPPE-flex[121] (flexible molecule version of TraPPE).[122]

In the MS-EVB approach, the reactive system is described by the Hamiltonian matrix $H(q)$

DOI: 10.1021/acs.jpca.9b08789
J. Phys. Chem. A 2019, 123, 10772−10781

$$H(q) = \begin{bmatrix} V_R + \varepsilon_R & H_{12} \\ H_{12} & V_P + \varepsilon_P \end{bmatrix} \quad (4)$$

where $\varepsilon_R = -48.0$ kcal/mol, $\varepsilon_P = 1.0$ kcal/mol for H···O, $\varepsilon_R = -63.0$ kcal/mol, and $\varepsilon_P = 1.0$ kcal/mol for O···O. These parameters represent constant diagonal energy shifts (subscripts R and P denote reactant and product, respectively). The diagonal elements V_R and V_P correspond to molecular mechanics energy of particular molecular states (Figure 1).

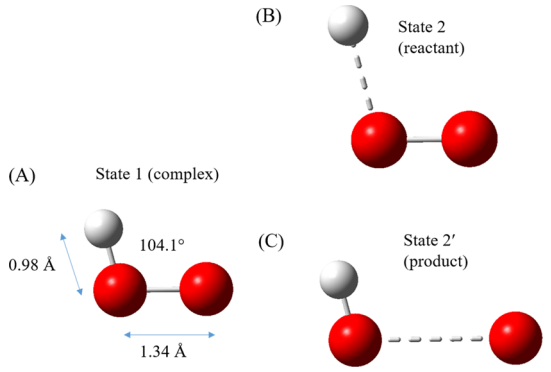

Figure 1. Schematic representation of the two states (reactant and product) in the MS-EVB model.

The off-diagonal $H_{12}(r_1,r_2)$ is fitted from the two-dimensional ellipsoidal Gaussian function

$$H_{12}(r_1, r_2) = A_{12} \exp(-a(r_1 - r_1^0)^2 + 2b(r_1 - r_1^0)(r_2 - r_2^0) + c(r_2 - r_2^0)^2) \quad (5)$$

where r_1 and r_2 are H−O or O−O bond distances in stable and transition states. $A_{12} = 25.0$ kcal/mol (for H−O) and 30 kcal/mol (for O−O). $r_1^0 = 1.0$ Å and $r_2^0 = 1.5$ Å (for both H−O and O−O) are the respective reference values of r_1 and r_2. a, b, and c are defined as

$$a = \frac{\cos^2\theta}{2\sigma_{r1}^2} + \frac{\sin^2\theta}{2\sigma_{r2}^2} \quad (6)$$

$$b = -\frac{\sin 2\theta}{4\sigma_{r1}^2} + \frac{\sin 2\theta}{4\sigma_{r2}^2} \quad (7)$$

$$c = \frac{\sin^2\theta}{2\sigma_{r1}^2} + \frac{\cos^2\theta}{2\sigma_{r2}^2} \quad (8)$$

where θ is Gaussian rotation angle $\sigma_{r1} = 5.0$ and $\sigma_{r2} = 5.0$ (for both H−O and O−O) are the respective widths in r_1 and r_2 directions. The purpose of fitting these parameters, the shifted energy ε, the amplitude A, the center r^0, and the width σ_r, is to adjust two one-dimensional PESs to reproduce PESs by Walch et al.[51−53] Figure S1 in Supporting Information shows MS-EVB-fitted PESs in comparison with the Walch results.

We used the following MD protocol. A Nosé−Hoover[123,124] thermostat was applied for constant volume and constant temperature ensemble (NVT) in accordance with the velocity-Verlet integrator. A time step of 0.2 fs was adopted to appropriately describe hydrogen atom motions. Simulations were performed under periodic boundary conditions in 26.0 × 26.0 × 26.0 Å^3 box with particle mesh Ewald[125,126] summation to better estimate long-range interactions. One HO_2 molecule and N CO_2 molecules (N = 0, 2, 4, 8, 16, 32, and 77) were included in a simulation box. T = 1000, 1200, 1400, 1600, 1800, and 2000 K were selected for the simulation. For US setup, the reaction coordinates are split to 31 windows from 0.5 to 8.0 Å (for H−O) and 0.75 to 8.25 Å (for O−O) so that each window is 0.05 Å wide. Bias force constant was assigned a value of 80.0 kcal/mol/Å^2 because strong constraint was found necessary in this simulation system. The trajectories were propagated for 5.0 ns to equilibrate the simulation system, and then followed by 5.0 ns production run. WHAM program[101] was used to assemble the continuous PMF curve.

3. RESULTS AND DISCUSSION

3.1. Potential Energy Surfaces for H + O_2 ⇌ HO_2 ⇌ HO + O. The reaction pathway of R1 was obtained by ab initio calculations in the gas phase, as shown in Figure 2. In this

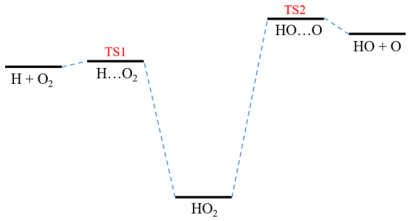

Figure 2. Schematic reaction path of the reactive system CCSD(T)/aug-cc-pVQZ theory level + ZPE at the CCSD/cc-pVDZ theory level.

study, the TS1 was found to have an H···O distance of 1.76 Å and an H···O−O angle of 114.8°, and for TS2, the distance O···O was 2.78 Å and O···O−H angle of 66.6°. The bond length and the angle of the intermediate is presented in state 1 (complex), as shown in Figure 1. The reaction pathway also shows the difficulty of the application of TST because the long-lived complex HO_2 will violate the assumption of direct dynamics in TS.[95] Calculated ab initio energies for TS1 and TS2 were corrected empirically so that the RRKM predictions of the pressure-dependent R1 and R2 reaction rates agree with experimental low and high pressure rate constants included in the shock tube experiment at 1.83−2.66 atm.[18] The corrected and uncorrected values for TS1 and TS2 energies are listed in Table 1 along with those for reactants, intermediate, and products. The 0.5 kcal/mol correction to TS1 energy and 2.5 kcal/mol correction to TS2 energy appear to be necessary to obtain the experimentally measured rates using the application of the RRKM theory.

Table 1. Potential Energy Surface of the Reactants, TS1, Intermediate, TS2, and Products[a]

	CCSD(T)/aug-cc-pVQZ//CCSD/cc-pVDZ	
	corrected	original
reactants	47.86	47.86
TS1	48.39	47.90
intermediate	0.00	0.00
TS2	64.08	61.61
products	62.68	62.68

[a]Intermediate is set to zero. The unit of energy is kcal/mol.

The reactions in sCO_2 environment was simulated at various densities (numbers of CO_2 molecules) by MDs simulation in an NVT ensemble. Figure 3 shows the representative snapshots of HO_2 molecules in the sCO_2 environment.

DOI: 10.1021/acs.jpca.9b08789
J. Phys. Chem. A 2019, 123, 10772−10781

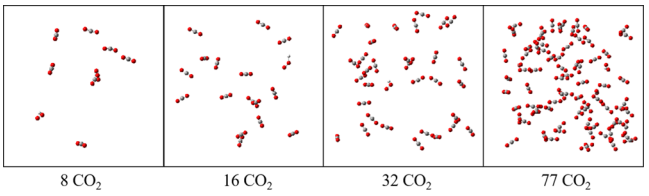

Figure 3. Representative snapshot of the HO_2 intermediate surrounded by 8, 16, 32, and 77 CO_2 molecules.

The calculations of the rate constant k were performed in several steps as follows. After the determination of PES (Figure S1), the MD trajectory was generated for each umbrella sampling window. Next, a WHAM was used to analyze these trajectories and produce PMF. In turn, these PMFs were used to determine the activation free energy of the reactions. Finally, the changes in activation energies between low and high pressure conditions are added to the ab initio energies of the transition states used in TST and RRKM calculations to take into account the solvation effects.

Sample PMFs for the two reactions $HO_2 \rightleftharpoons H + O_2$ and $HO_2 \rightleftharpoons HO + O$ are shown in Figure S2 in Supporting Information. Table S1 presents the pressures at specific densities and temperatures. It shows that at $N = 8$ and $T = 1200$ K, the simulation reaches the supercritical CO_2 state (>72.9 atm). The increase of temperature leads to the decrease of energy barrier for R2r (Table S3) and R3r (Table S5), while increasing the energy barrier for R2 (Table S4). From Figure S2, we were able to calculate ΔG_{sol} of R2, R2r, and R3r for further calculation of $\Delta G^{\ddagger}$. In the RRKM theory, it is not necessary to calculate ΔG_{sol} of R3, and it is not shown here. Table S2 lists branching fractions f_1 (backward reaction R1r), f_2 (forward reaction R1), and f_{stab} (stabilization reaction R2) of HO_2 reaction calculated by the RRKM theory.

To fit ΔG_{sol} into the assigned pressure, we applied exponential and biexponential least-square fitting for R2 (exponential), R2r, and R3r (bi-exponential) because the increase of free energy is not linear as N increases, and the parameters and ΔG_{sol} values are shown in Tables S3–S5. In R2r and R3r, as the pressure approaches 400 atm (below 1000 atm), the relation between pressure and activation energy is approximately linear. In R2, ΔG_{sol} decreases after 100 atm. At the end, $\Delta\Delta G_{sol}$ is obtained by ΔG_{sol}(pressure) − ΔG_{sol}(0 CO_2) and is added into $\Delta G^{\ddagger}$ according to eq 2 and the corrected free energy was used in RRKM theory to obtain k in pressure 100–400 atm.

3.2. $H + O_2 \rightleftharpoons HO + O$. Table 2 presents parameters of Arrhenius and extended Arrhenius equations between 1000 and 2000 K. The decreased activation energy as the pressure increases in the extended Arrhenius equation shows the decreased barrier of R1r reaction. . The absolute value for $|n|$ in the extended Arrhenius equation is less than 2 at 400 atm and does not improve the accuracy of the fit significantly compared to the Arrhenius equation ($n = 0$).

In Figure 4, k at 100–400 atm (this work) between 1000 and 2000 K is pressure independent. As the temperature increases, k increases monotonically. The consistency of branching fraction f_2 (forward reaction R1, see Table S2) at pressures from 100 to 400 atm demonstrates the pressure-independence of R1 as well. Measurements of reaction rates k at low pressures performed by a shock tube[19,26] (0.66–1.31 and 1.01–2.03 atm) and flash photolysis[24] (0.013–0.021 atm) experiments and theoretical flux–flux autocorrelation function methods[70] are shown in Figure 4 for comparison. Comparisons with the other experimental (shock tube, flash photolysis, etc) and theoretical (TST) results can be found in Tables S6a–c (see Supporting Information). Because R1 is pressure-independent, k is consistent at different pressures performed experimentally and theoretically, and our results are close to that predicted by TST,[70] and measured by flash photolysis[24] and shock tube experiments.[19,26] The rate constant at 300 atm predicted in this work is $4.23 \times 10^{-7}\ T^{-0.73}\ \exp(-21\,855.2\ \text{cal/mol/RT})$ cm^3/molecule/s.

3.3. $H + O_2 \rightleftharpoons HO_2$. Our rate predictions for reaction R2 are reported in Table 3. When $n = 0$ (Arrhenius form), E_a shows the barrierless nature of the decreased rate as temperature increases. This happens when the increasing temperature decreases the probability of collision of reactants as the increased momentum carries the reactants away from the collision zone. However, when $|n| > 0$ (extended Arrhenius form), all of $|n|$ values are between 2.0 and 3.0 and the reaction is characterized by positive activation energy. Because of the position of H···O_2 (TS1, see Figure 1), $|n| > 0$ is more accurate because there is a barrier between H + O_2 and HO_2, and $|n| > 0$ will be considered in the following discussion.

Figure 5 (see Tables S7a–b as well for more detail) presents the Arrhenius plot of the rate constant for reaction R2 and illustrates the disagreement of the high-pressure limit, obtained with different theoretical (TST[27,83,85] and RRKM[30,85]) methods. In this work, the rate constant of reaction R2 is calculated by TST first, which means R2 is the complete reaction, where HO_2 is the only product without products HO and O (such as R1 reaction). Rate constants k of R2 are presented in Table S8 in Supporting Information. As the temperature increases, k increases slightly (from 7.22×10^{-11} to 1.41×10^{-10} cm^3/molecule/s, high-pressure limit) and the result agrees with Sellevåg et al.[83] and Duchovic et al.[85] (see Figure 5). Based upon Fernandes et al. results,[33] rate constant at the high-pressure limit ($\sim 10^{-11}$) agrees with our calculated k at specific pressure and (i) k slightly decreases as the temperature increases; (ii) k increases as the pressure increases (more collision between HO_2 and bath gas CO_2). Furthermore, branching fraction by RRKM (Table S2 in Supporting Information) explains the significant decrease in the ratio of stabilization reaction (f_{stab}, which represents lower

Table 2. Fitted Arrhenius Equation and the Extended Arrhenius Equation of k of R1 between 1000 and 2000 K

		Arrhenius equation				extended Arrhenius equation			
		pressure (atm)				pressure (atm)			
		100	200	300	400	100	200	300	400
A	cm^3/molecule/s	1.06×10^{-9}	1.04×10^{-9}	9.85×10^{-10}	9.67×10^{-10}	6.25×10^{-4}	1.48×10^{-5}	4.23×10^{-7}	4.10×10^{-8}
n		0	0	0	0	−1.61	−1.16	−0.73	−0.45
E_a	cal/mol	19 946.4	20 077.3	19 844.1	19 697.3	24 354.4	23 249.0	21 855.2	20 940.0

DOI: 10.1021/acs.jpca.9b08789
J. Phys. Chem. A 2019, 123, 10772–10781

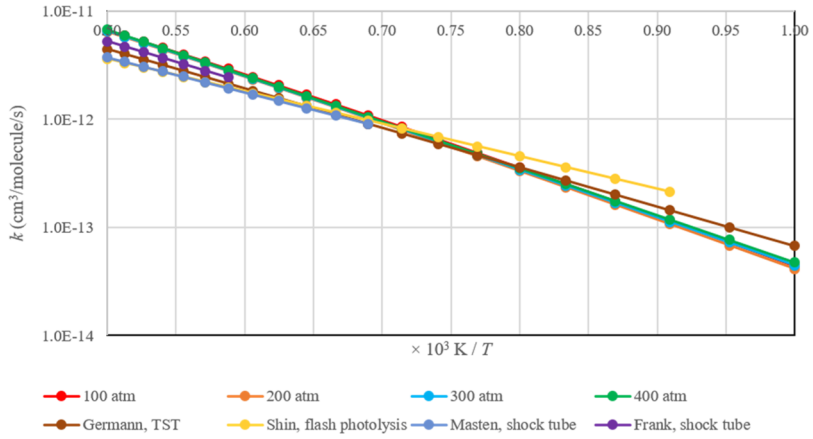

Figure 4. Arrhenius plot of rate constant k of R1 (cm^3/molecule/s) reaction in 100−400 atm (this work) in comparison with other experiments[19,24,26] and theory[70] that the pressure is lower than 2 atm.

Table 3. Fitted Arrhenius Equation and the Extended Arrhenius Equation of k of R2 between 1000 and 2000 K

		Arrhenius equation				extended Arrhenius equation			
		pressure (atm)				pressure (atm)			
		100	200	300	400	100	200	300	400
A	cm^3/molecule/s	1.05×10^{-12}	2.04×10^{-12}	2.85×10^{-12}	3.67×10^{-12}	5.81×10^{1}	9.66×10^{-1}	5.22×10^{-2}	2.76×10^{-3}
n		0	0	0	0	−3.83	−3.26	−2.86	−2.47
E_a	cal/mol	−1028.4	−574.4	−591.2	−578.1	9467.2	8342.4	7247.4	6200.8

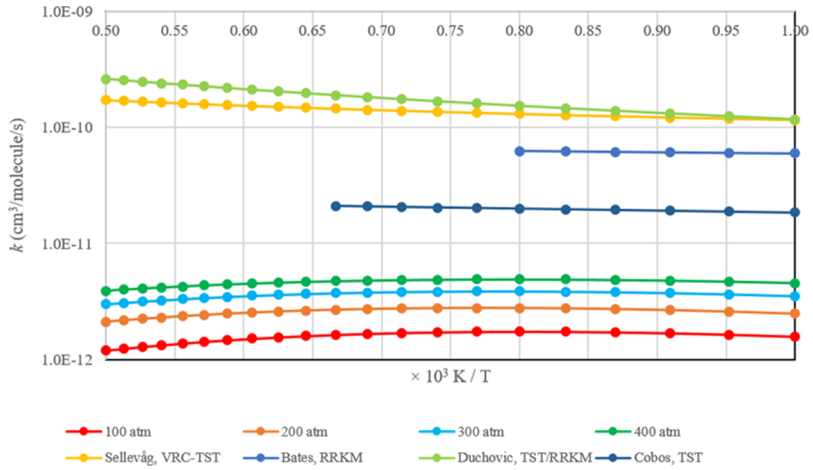

Figure 5. Arrhenius plot of rate constant k of R2 (cm^3/molecule/s) reaction in 100−400 atm (this work) in comparison with other theoretical studies[30,83,85,94] at a high-pressure limit.

k of reaction R2 in this case) leads to decreased k as temperature increases. After correction by the RRKM theory, the k increases with the pressure and approaches the high-pressure limit as expected. Our results agree that the increase of k with increased pressure from 100 to 400 atm, which is close to k evaluated from the high-pressure limit by theoretical methods TST[83,85,94] and RRKM.[30,85] The rate constant at 300 atm is $5.22 \times 10^{-2}\ T^{-2.86}\ \exp(-7247.4\ \text{cal/mol/RT})$ cm^3/molecule/s.

4. CONCLUSIONS

We evaluated the rate constants for the reactions R1 and R2 between a hydrogen atom and an oxygen molecule in a supercritical CO_2 environment and its Arrhenius parameters. These reaction are among the most important reactions in hydrocarbon combustion mechanism. To accurately evaluate k of these reactions, high-level quantum chemical calculations were performed at the CCSD(T)/aug-cc-pVQZ//CCSD/cc-pVDZ theory level to calculate the rate constant of R2 in the gas phase by TST first. Classical MD simulations were performed to study the dynamics of chemical reactions with explicit CO_2 molecules included in conjunction with the MS-EVB method to reproduce potential energy of free radical reactions. TST was applied to calculate k of R2, followed by the RRKM method to calculate k of R1 and R2 at high pressures from 100 to 400 atm. The rate constant of reaction R1 was found to be pressure-independent between 100 and 400 atm in bimolecular reaction with only one product and is two orders of magnitude lower than that at ambient pressure. The rate constant of reaction R1 at 300 atm was found to be $4.23 \times 10^{-7}\ T^{-0.73}\ \exp(-21\,855.2\ \text{cal/mol/RT})$ cm^3/molecule/s. The rate constant of reaction R2 demonstrates

DOI: 10.1021/acs.jpca.9b08789
J. Phys. Chem. A 2019, 123, 10772−10781

pressure-dependence between 100 and 400 atm and increases with the pressure. The rate constant of reaction R2 at 300 atm was found to be $5.22 \times 10^{-2}\ T^{-2.86}\ \exp(-7247.4\ \text{cal/mol/RT})\ \text{cm}^3/\text{molecule/s}$.

■ ASSOCIATED CONTENT

Supporting Information

The Supporting Information is available free of charge at https://pubs.acs.org/doi/10.1021/acs.jpca.9b08789.

Energy surface, PMF, calculated density and pressure of the MD simulation, the fitted free energy corresponding to various pressures, and rate constants at various temperatures (PDF)

■ AUTHOR INFORMATION

Corresponding Authors

*E-mail: amasunov@ucf.edu (A.E.M.).
*E-mail: subith@ucf.edu (S.S.V.).

ORCID

Artëm E. Masunov: 0000-0003-4924-3380
Subith S. Vasu: 0000-0002-4164-3163

Notes

The authors declare no competing financial interest.

■ ACKNOWLEDGMENTS

This material is based upon the work supported by the KEPCO Research Institute (KEPRI), Hanwha Power Systems (HPS), and Southwest Research Institute (SwRI). The partial financial support from the UCF College of Graduate Studies is appreciated. We thank K. R. V. Manikantachari for helpful discussion about the importance of combustion reaction in the supercritical environment. The authors acknowledge the National Energy Research Scientific Computing Center (NERSC) and the UCF Advanced Research Computing Center (https://arcc.ist.ucf.edu) for providing computational resources and support. A.E.M. acknowledges the support by the Act 211 Government of the Russian Federation (contract no. 02.A03.21.0011) and by the "improving of the competitiveness" program of the National Research Nuclear University MEPhI.

■ REFERENCES

(1) Miller, J. A.; Pilling, M. J.; Troe, J. Unravelling combustion mechanisms through a quantitative understanding of elementary reactions. *Proc. Combust. Inst.* **2005**, *30*, 43−88.

(2) Allam, R.; Martin, S.; Forrest, B.; Fetvedt, J.; Lu, X.; Freed, D.; Brown, G. W., Jr.; Sasaki, T.; Itoh, M.; Manning, J. Demonstration of the Allam Cycle: An Update on the Development Status of a High Efficiency Supercritical Carbon Dioxide Power Process Employing Full Carbon Capture. *Energy Procedia* **2017**, *114*, 5948−5966.

(3) Allam, R. J.; Fetvedt, J. E.; Forrest, B. A.; Freed, D. A. The Oxy-Fuel, Supercritical CO_2 Allam Cycle: New Cycle Developments to Produce Even Lower-Cost Electricity From Fossil Fuels Without Atmospheric Emissions. *3B: Oil and Gas Applications; Organic Ranking Cycle Power Systems; Supercritical CO_2 Power Cycles; Wind Energy*, Turbo Expo: Power for Land, Sea, and Air 2014; The American Society of Mechanical Engineers, 2014; V03BT36A016.

(4) Manikantachari, K. R. V.; Martin, S.; Bobren-Diaz, J. O.; Vasu, S. S. Thermal and Transport Properties for the Simulation of Direct-Fired sCO_2 Combustor. *J. Eng. Gas Turbines Power* **2017**, *139*, 121505.

(5) Manikantachari, K. R. V.; Vesely, L.; Martin, S.; Bobren-Diaz, J. O.; Vasu, S. S. Reduced Chemical Kinetic Mechanisms for Oxy/Methane Supercritical CO_2 Combustor Simulations. *J. Energy Resour. Technol.* **2018**, *140*, 092202.

(6) Manikantachari, K. R. V.; Martin, S.; Rahman, R. K.; Velez, C.; Vasu, S. S. In A General Study of Counterflow Diffusion Flames for Supercritical CO_2 Mixtures. *Proceedings of the ASME Turbo Expo 2019: Turbomachinery Technical Conference & Exposition*, Phoenix, AZ, 2019; p GT2019-90332.

(7) Masunov, A. E.; Atlanov, A. A.; Vasu, S. S. Molecular Dynamics Study of Combustion Reactions in a Supercritical Environment. Part 1: Carbon Dioxide and Water Force Field Parameters Refitting and Critical Isotherms of Binary Mixtures. *Energy Fuels* **2016**, *30*, 9622−9627.

(8) Masunov, A. E.; Wait, E.; Vasu, S. S. Quantum Chemical Study of $CH_3 + O_2$ Combustion Reaction System: Catalytic Effects of Additional CO_2 Molecule. *J. Phys. Chem. A* **2017**, *121*, 5681−5689.

(9) Masunov, A. E.; Wait, E. E.; Atlanov, A. A.; Vasu, S. S. Quantum Chemical Study of Supercritical Carbon Dioxide Effects on Combustion Kinetics. *J. Phys. Chem. A* **2017**, *121*, 3728−3735.

(10) Masunov, A. E.; Atlanov, A. A.; Vasu, S. S. Potential Energy Surfaces for the Reactions of HO_2 Radical with CH_2O and HO_2 in CO_2 Environment. *J. Phys. Chem. A* **2016**, *120*, 7681−7688.

(11) Masunov, A. E.; Wait, E.; Vasu, S. S. Chemical Reaction CO +OH• → CO_2+H• Autocatalyzed by Carbon Dioxide: Quantum Chemical Study of the Potential Energy Surfaces. *J. Phys. Chem. A* **2016**, *120*, 6023−6028.

(12) Panteleev, S. V.; Masunov, A. E.; Vasu, S. S. Molecular Dynamics Study of Combustion Reactions in a Supercritical Environment. Part 2: Boxed MD Study of CO + OH → CO_2 + H Reaction Kinetics. *J. Phys. Chem. A* **2018**, *122*, 897−908.

(13) Panteleev, S. V.; Masunov, A. E.; Vasu, S. S. Molecular Dynamics Study of Combustion Reactions in Supercritical Environment. Part 3: Boxed MD Study of $CH_3 + HO_2$ → CH_3O + OH Reaction Kinetics. *J. Phys. Chem. A* **2018**, *122*, 3337−3345.

(14) Panteleev, S. V.; Masunov, A. E.; Vasu, S. S. Molecular dynamics of combustion reactions in supercritical carbon dioxide. Part 4: boxed MD study of formyl radical dissociation and recombination. *J. Mol. Model.* **2019**, *25*, 35.

(15) Wang, C.-H.; Panteleev, S. V.; Masunov, A. E.; Allison, T. C.; Chang, S.; Lim, C.; Jin, Y.; Vasu, S. S. Molecular Dynamics of Combustion Reactions in Supercritical Carbon Dioxide. Part 5: Computational Study of Ethane Dissociation and Recombination Reactions $C_2H_6 \rightleftharpoons CH_3 + CH_3$. *J. Phys. Chem. A* **2019**, *123*, 4776−4784.

(16) Wait, E. E.; Masunov, A. E.; Vasu, S. S. Quantum chemical and master equation study of OH + CH_2O → H_2O + CHO reaction rates in supercritical CO_2 environment. *Int. J. Chem. Kinet.* **2019**, *51*, 42−48.

(17) Masunov, A. E.; Wait, E. E.; Vasu, S. S. Catalytic Effect of Carbon Dioxide on Reaction OH + CO → H + CO_2 in Supercritical Environment: Master Equation Study. *J. Phys. Chem. A* **2018**, *122*, 6355−6359.

(18) Hong, Z.; Davidson, D. F.; Barbour, E. A.; Hanson, R. K. A new shock tube study of the H + O_2 → OH + O reaction rate using tunable diode laser absorption of H_2O near 2.5 μm. *Proc. Combust. Inst.* **2011**, *33*, 309−316.

(19) Masten, D. A.; Hanson, R. K.; Bowman, C. T. Shock Tube Study of the Reaction H + O_2 → OH + O Using OH Laser Absorption. *J. Phys. Chem.* **1990**, *94*, 7119−7128.

(20) Hwang, S. M.; Ryu, S.-O.; Witt, K. J. D.; Rabinowitz, M. J. High temperature rate coefficient measurements of H + O_2 chain-branching and chain-terminating reaction. *Chem. Phys. Lett.* **2005**, *408*, 107−111.

(21) Yu, C.-L.; Frenklach, M.; Masten, D. A.; Hanson, R. K.; Bowman, C. T. Reexamination of Shock-Tube Measurements of the Rate Coefficient of H + O_2 → OH + O. *J. Phys. Chem.* **1994**, *98*, 4770−4771.

(22) Du, H.; Hessler, J. P. Rate coefficient for the reaction H + O_2 → OH + O: Results at high temperatures, 2000 to 5300 K. *J. Chem. Phys.* **1992**, *96*, 1077−1092.

DOI: 10.1021/acs.jpca.9b08789
J. Phys. Chem. A 2019, 123, 10772−10781

(23) Yuan, T.; Wang, C.; Yu, C. L.; Frenklach, M.; Rabinowitz, M. J. Determination of the Rate Coefficient for the Reaction H + O_2 → OH + O by a Shock Tube/Laser Absorption/Detailed Modeling Study. *J. Phys. Chem.* **1991**, *95*, 1258−1265.
(24) Shin, K. S.; Michael, J. V. Rate constants for the reactions H + O_2 → OH + O and D + O_2 → OD + O over the temperature range 1085-2278 K by the laser photolysis-shock tube technique. *J. Chem. Phys.* **1991**, *95*, 262−273.
(25) Pirraglia, A. N.; Michael, J. V.; Sutherland, J. W.; Klemm, R. B. A Flash Photolysis-Shock Tube Kinetic Study of the H Atom Reaction with O_2: H + O_2 ⇌ OH + O (962 K ≤ T ≤ 1705 K) and H + O_2 + Ar → HO_2 + Ar (746 K ≤ T ≤ 987 K). *J. Phys. Chem.* **1989**, *93*, 282−291.
(26) Frank, P.; Just, T. High Temperature Reaction Rate for H + O_2 = OH + O and OH + H_2 = H_2O + H. *Ber. Bunsenges. Phys. Chem.* **1985**, *89*, 181−187.
(27) Cobos, C. J.; Hippler, H.; Troe, J. High-Pressure Falloff Curves and Specific Rate Constants for the Reactions H + O_2 ⇌ HO_2 ⇌ HO + O. *J. Phys. Chem.* **1985**, *89*, 342−349.
(28) Mertens, J. D.; Kalitan, D. M.; Barrett, A. B.; Petersen, E. L. Determination of the rate of H + O_2 + M → HO_2 + M (M = N_2, Ar, H_2O). *Proc. Combust. Inst.* **2009**, *32*, 295−303.
(29) Michael, J. V.; Su, M.-C.; Sutherland, J. W.; Carroll, J. J.; Wagner, A. F. Rate Constants For H + O_2 + M → HO_2 + M in Seven Bath Gases. *J. Phys. Chem. A* **2002**, *106*, 5297−5313.
(30) Bates, R. W.; Golden, D. M.; Hanson, R. K.; Bowman, C. T. Experimental study and modeling of the reaction H + O_2 + M → HO_2 + M (M = Ar, N_2, H_2O) at elevated pressures and temperatures between 1050 and 1250 K. *Phys. Chem. Chem. Phys.* **2001**, *3*, 2337−2342.
(31) Shao, J.; Choudhary, R.; Susa, A.; Davidson, D. F.; Hanson, R. K. Shock tube study of the rate constants for H + O_2 + M → HO_2 + M (M = Ar, H_2O, CO_2, N_2) at elevated pressures. *Proc. Combust. Inst.* **2019**, *37*, 145−152.
(32) Hahn, J.; Krasnoperov, L.; Luther, K.; Troe, J. Pressure dependence of the radiion H + O_2 (+Ar) → HO_2 (+Ar) in the range 1-900 bar and 300-700 K. *Phys. Chem. Chem. Phys.* **2004**, *6*, 1997−1999.
(33) Fernandes, R. X.; Luther, K.; Troe, J.; Ushakov, V. G. Experimental and modelling study of the recombination reaction H + O_2 (+M) → HO_2 (+M) between 300 and 900 K, 1.5 and 950 bar, and in the bath gases M = He, Ar, and N_2. *Phys. Chem. Chem. Phys.* **2008**, *10*, 4313−4321.
(34) Mueller, M. A.; Yetter, R. A.; Dryer, F. L. Measurement of the rate constant for H + O_2 + M → HO_2 + M (M = N_2, Ar) using kinetic modeling of the high-pressure $H_2/O_2/NO_x$ reaction. *Proc. Combust. Inst.* **1998**, *27*, 177−184.
(35) Janik, I.; Bartels, D. M.; Marin, T. W.; Jonah, C. D. Reaction of O_2 with the Hydrogen Atom in Water up to 350 °C. *J. Phys. Chem. A* **2007**, *111*, 79−88.
(36) Bao, J. L.; Truhlar, D. G. Variational transition state theory: theoretical framework and recent developments. *Chem. Soc. Rev.* **2017**, *46*, 7548−7596.
(37) Varandas, A. J. C. Accurate combined-hyperbolic-inverse-power-representation of ab initio potential energy surface for the hydroperoxyl radical and dynamics study of O + OH reaction. *J. Chem. Phys.* **2013**, *138*, 134117.
(38) Varandas, A. J. C. Combined-hyperbolic-inverse-power-representation of potential energy surfaces: A preliminary assessment for H_3 and HO_2. *J. Chem. Phys.* **2013**, *138*, 054120.
(39) Xu, C.; Xie, D.; Zhang, D. H.; Lin, S. Y.; Guo, H. A new ab initio potential-energy surface of $HO_2(X^2A'')$ and quantum studies of HO_2 vibrational spectrum and rate constants for the H + O_2 ↔ O + OH reactions. *J. Chem. Phys.* **2005**, *122*, 244305.
(40) Ma, J.; Lin, S. Y.; Guo, H.; Sun, Z.; Zhang, D. H.; Xie, D. State-to-state quantum dynamics of the $O(P_3)$ + $OH(\Pi_2)$ → $H(S_2)$ + $O_2(\Sigma_3 g^-)$ reaction. *J. Chem. Phys.* **2010**, *133*, 054302.
(41) Lin, S. Y.; Guo, H.; Honvault, P.; Xie, D. Quantum Dynamics of the H + O_2 → O + OH Reaction on an Accurate ab initio Potential Energy Surface. *J. Phys. Chem. B* **2006**, *110*, 23641−23643.
(42) Kendrick, B.; Pack, R. T. Potential energy surfaces for the low-lying 2A″ and 2A' States of HO_2: Use of the diatomics in molecules model to fit ab initio data. *J. Chem. Phys.* **1995**, *102*, 1994−2012.
(43) Quéméner, G.; Balakrishnan, N.; Kendrick, B. K. Formation of molecular oxygen in ultracold O + OH collisions. *Phys. Rev. A* **2009**, *79*, 022703.
(44) Quéméner, G.; Balakrishnan, N.; Kendrick, B. K. Quantum dynamics of the O + OH → H + O_2 reaction at low temperatures. *J. Chem. Phys.* **2008**, *129*, 224309.
(45) Xie, D.; Xu, C.; Ho, T.-S.; Rabitz, H.; Lendvay, G.; Lin, S. Y.; Guo, H. Global analytical potential energy surfaces for $HO_2(X^2A'')$ based on high-level ab initio calculations. *J. Chem. Phys.* **2007**, *126*, 074315.
(46) Pastrana, M. R.; Quintales, L. A. M.; Brandao, J.; Varandas, A. J. C. Recalibration of a Single-Valued Double Many-Body Expansion Potential Energy Surface for Ground-State HO_2 and Dynamics Calculations for the O + OH → O_2 + H Reaction. *J. Phys. Chem.* **1990**, *94*, 8073−8080.
(47) Brandão, J.; Rio, C. M. A.; Tennyson, J. A modified potential for HO_2 with spectroscopic accuracy. *J. Chem. Phys.* **2009**, *130*, 134309.
(48) Melius, C. F.; Blint, R. J. The Potential Energy Surface of the HO_2 Molecular System. *Chem. Phys. Lett.* **1979**, *64*, 183−189.
(49) Klimo, V.; Bittererová, M.; Biskupič, S.; Urban, J. Quasiclassical trajectory study of H + O_2 → OH + O at temperatures from 500 to 2000 K. *Chem. Phys.* **1993**, *173*, 367−375.
(50) Lemon, W. J.; Hase, W. L. A Potential Energy Function for the Hydroperoxyl Radical. *J. Phys. Chem.* **1987**, *91*, 1596−1602.
(51) Walch, S. P.; Rohlfing, C. M.; Melius, C. F.; Bauschlicher, C. W., Jr. Theoretical characterization of the minimum energy path for the reaction H + O_2 → HO_2* → HO + O. *J. Chem. Phys.* **1988**, *88*, 6273−6281.
(52) Walch, S. P.; Rohlfing, C. M. Theoretical characterization of the potential energy surface for H + O_2 → HO_2* → HO + O. II. The potential for H atom exchange in HO_2. *J. Chem. Phys.* **1989**, *91*, 2373−2375.
(53) Walch, S. P.; Duchovic, R. J. Theoretical characterization of the potential energy surface for H + O_2 ⇌ HO_2* ⇌ OH + O. III. Computed points to define a global potential energy surface. *J. Chem. Phys.* **1991**, *94*, 7068−7075.
(54) Xu, C.; Xie, D.; Honvault, P.; Lin, S. Y.; Guo, H. Rate constant for $OH(^2\Pi)$ + $O(^3P)$ → $H(^2S)$ + $O_2(^3\Sigma g^-)$ reaction on an improved ab initio potential energy surface and implications for the interstellar oxygen problem. *J. Chem. Phys.* **2007**, *127*, 024304.
(55) Li, A.; Xie, d.; Dawe, R.; Ajsper, A. M.; Ma, J.; Guo, H. Global protential energy surface, vibrational spectrum, and reaction dynamics of the first excited $(\tilde{A}^2A')$ state of HO_2. *J. Chem. Phys.* **2010**, *133*, 144306.
(56) Teixidor, M. M.; Varandas, A. J. C. Quantum dynamics study of the X + O_2 reactions on the CHIPR potential energy surface: X = Mu, H, D, T. *Chem. Phys. Lett.* **2015**, *638*, 61−65.
(57) Teixidor, M. M.; Varandas, A. J. C. Quantum dynamics study on the CHIPR potential energy surface for the hydroperoxyl radical: The reactions O + OH ⇌ O_2 + H. *J. Chem. Phys.* **2015**, *142*, 014309.
(58) Lin, S. Y.; Rackham, E. J.; Guo, H. Quantum Mechanical Rate Constants for H + O_2 ⇌ O + OH and H + O_2 ⇌ HO_2 Reactions. *J. Phys. Chem. A* **2006**, *110*, 1534−1540.
(59) Teitelbaum, H.; Caridade, P. J. S. B.; Varandas, A. J. C. Calculation of the rate constant for state-selected recombination of H + O_2(v) as a function of temperature and pressure. *J. Chem. Phys.* **2004**, *120*, 10483−10500.
(60) Leforestier, C.; Miller, W. H. Quantum mechanical calculation of the rate constant for the reaction H + O_2 → HO + O. *J. Chem. Phys.* **1994**, *100*, 733−735.

DOI: 10.1021/acs.jpca.9b08789
J. Phys. Chem. A 2019, 123, 10772−10781

(61) Viel, A.; Leforestier, C.; Miller, W. H. Quantum mechanical calculation of the rate constant for the reaction H + O_2 → HO + O. *J. Chem. Phys.* **1998**, *108*, 3489−3497.
(62) Pradhan, G. B.; Juanes-Marcos, J. C.; Balakrishnan, N.; Kendrick, B. K. Chemical reaction versus vibrational quenching in low energy collisions of vibrationally excited OH with O. *J. Chem. Phys.* **2013**, *139*, 194305.
(63) Harding, L. B.; Maergoiz, A. I.; Troe, J.; Ushakov, V. G. Statistical rate theory for the HO + O ⇌ HO_2 ⇌ H + O_2 reaction system: SACM/CT calculations between 0 and 5000 K. *J. Chem. Phys.* **2000**, *113*, 11019−11034.
(64) Troe, J.; Ushakov, V. G. Theoretical studies of the HO + O ⇌ HO_2 ⇌ H + O_2 reaction. II. Classical trajectory calculations on an ab initio potential for temperatures between 300 and 5000 K. *J. Chem. Phys.* **2001**, *115*, 3621−3628.
(65) Kłoz, J. A.; Lique, F.; Alexander, M. H.; Dagdigian, P. J. Theoretical determination of rate constants for vibrational relaxation and reaction of OH($X^2\Pi$,v=1) with O(^{3}P) atoms. *J. Chem. Phys.* **2008**, *129*, 064306.
(66) Issacson, A. D.; Truhlar, D. G. Polyatomic canonical variational theory for chemical reaction rates. Separable-mode formalism with application to OH + H_2 → H_2O + H. *J. Chem. Phys.* **1982**, *76*, 1380−1391.
(67) Miller, J. A.; Garrett, B. C. Quantifying the non-RRKM effect in the H + O_2 ⇌ OH + O reaction. *Int. J. Chem. Kinet.* **1997**, *29*, 275−287.
(68) Rai, S. N.; Truhlar, D. G. Variational transition state theory calculations for an atom-radical reaction with no saddle point: O + OH. *J. Chem. Phys.* **1983**, *79*, 6046−6059.
(69) Yang, C. Y.; Klippenstein, S. J. Comparisons between statistics, dynamics, and experiment for the H + O_2 → OH + O reaction. *J. Chem. Phys.* **1995**, *103*, 7287−7298.
(70) Germann, T. C.; Miller, W. H. Quantum Mechanical Pressure-Dependent Reaction and Recombination Rates for O + OH → H + O_2, HO_2. *J. Phys. Chem. A* **1997**, *101*, 6358−6367.
(71) Lique, F.; Jorfi, M.; Honvault, P.; Halvick, P.; Lin, S. Y.; Guo, H.; Xie, D. Q.; Dagdigian, P. J.; Kłos, J.; Alexander, M. H. O + OH → O_2 + H: A key reaction for interstellar chemistry. New theoretical results and comparison with experiment. *J. Chem. Phys.* **2009**, *131*, 221104.
(72) Jorfi, M.; Honvault, P.; Bargueño, P.; González-Lezana, T.; Larrégaray, P.; Bonnet, L.; Halvick, P. On the statistical behavior of the O + OH → H + O_2 reaction: A comparison between quasiclassical trajectory, quantum scattering, and statistical calculations. *J. Chem. Phys.* **2009**, *130*, 184301.
(73) Varandas, A. J. C.; Brandão, J.; Pastrana, M. R. Quasiclassical trajectory calculations of the thermal rate coefficients for the reactions H(D) + O_2 → OH(D) + O and O + OH(D) → O_2 + H(D) as a function of temperature. *J. Chem. Phys.* **1992**, *96*, 5137−5150.
(74) Duchovic, R. J.; Parker, M. A. A Quasiclassical Trajectory Study of the Reaction H + O_2 ⇌ OH + O with the O_2 Reagent Vibrationally Excited. *J. Phys. Chem. A* **2005**, *109*, 5883−5896.
(75) Miller, J. A. Nonstatistical effects and detailed balance in quasiclassical trajectory calculations of the thermal rate coefficient for O + OH → O_2 + H. *J. Chem. Phys.* **1986**, *84*, 6170−6177.
(76) Jorfi, M.; Honvault, P.; Halvick, P.; Lin, S. Y.; Guo, H. Quasiclassical trajectory scattering calculations for the OH + O → H + O_2 reaction: Cross sections and rate constants. *Chem. Phys. Lett.* **2008**, *462*, 53−57.
(77) Lendvay, G.; Xie, D.; Guo, H. Mechanistic insights into the H + O_2 → OH + O reaction from quasi-classical trajectory studies on a new ab initio potential energy surface. *Chem. Phys.* **2008**, *349*, 181−187.
(78) Bargueño, P.; González-Lezana, T.; Larrégaray, P.; Bonnet, L.; Rayez, J.-C.; Hankel, M.; Smith, S. C.; Meijer, A. J. H. M. Study of the H + O_2 reaction by means of quantum mechanical and statistical approaches: The dynamics on two different potential energy surfaces. *J. Chem. Phys.* **2008**, *128*, 244308.
(79) Hankel, M.; Smith, S. C.; Meijer, A. J. H. M. State-to-state reaction probabilities for the H + O_2(v,j) → O + OH(v',j') reaction on three potential energy surfaces. *J. Chem. Phys.* **2007**, *127*, 064316.
(80) Osborn, D. L. Reaction Mechanisms on Multiwell Potential Energy Surfaces in Combustion (and Atmospheric) Chemistry. *Annu. Rev. Phys. Chem.* **2017**, *68*, 233−260.
(81) Harding, L. B.; Klippenstein, S. J.; Lischka, H.; Sphepard, R. Comparison of multireference configuration interaction potential energy surfaces for H + O_2 → HO_2: the effect of internal extraction. *Theor. Chem. Acc.* **2014**, *133*, 1429.
(82) Harding, L. B.; Troe, J.; Ushakov, V. G. Classical trajectory calculations of the high pressure limiting rate constants and of specific rate constants for the reaction H + O_2 → HO_2: dynamic isotope effects between tritium + O_2 and muonium + O_2. *Phys. Chem. Chem. Phys.* **2000**, *2*, 631−642.
(83) Sellevåg, S. R.; Georgievskii, Y.; Miller, J. A. The Temperature and Pressure Dependence of the Reactions H + O_2 (+M) → HO_2 (+M) and H + OH (+M) → H_2O (+M). *J. Phys. Chem. A* **2008**, *112*, 5085−5095.
(84) Himmer, U.; Roduner, E. The addition reaction of X to O_2 (X = Mu, H, D): isotope effects in intra- and intermolecular energy transfer. *Phys. Chem. Chem. Phys.* **2000**, *2*, 339−347.
(85) Duchovic, R. J.; Pettigrew, J. D.; Welling, B.; Shipchandler, T. Conventional transition state theory/Rice-Ramsperger-Kassel-Marcus theory calculations of thermal termolecular rate coefficients for H(D) + O_2 + M. *J. Chem. Phys.* **1996**, *105*, 10367−10379.
(86) Dobbyn, A. J.; Stumpf, M.; Keller, H. M.; Hase, W. L.; Schinke, R. Quantum mechanical study of the unimolecular dissociation of HO_2: A rigorous test of RRKM theory. *J. Chem. Phys.* **1995**, *102*, 5867−5870.
(87) Troe, J.; Ushakov, V. G. Quantum capture, adiabatic channel, and classical trajectory study of the high-pressure rate constant of the reaction H + O_2 → HO_2 between 0 and 5000 K. *J. Chem. Phys.* **2008**, *128*, 204307.
(88) Burke, M. P.; Song, R. Evaluating Mixture Rules for Multi-Component Pressure Dependence: H + O_2 (+M) = HO_2 (+M). *Proc. Combust. Inst.* **2017**, *36*, 245−253.
(89) Lin, S. Y.; Guo, H.; Honvault, P.; Xu, C.; Xie, D. Accurate quantum mechanical calculations of differential and integral cross sections and rate constant for the O + OH reaction using an ab initio potential energy surface. *J. Chem. Phys.* **2008**, *128*, 014303.
(90) Marques, J. M. C.; Varandas, A. J. C. On the high pressure rate constants for the H/Mu + O_2 addition reactions. *Phys. Chem. Chem. Phys.* **2001**, *3*, 505−507.
(91) Mandelshtam, V. A.; Taylor, H. S.; Miller, W. H. Collisional recombination reaction H + O_2 + M → HO_2 + M: Quantum mechanical study using filter diagonalization. *J. Chem. Phys.* **1996**, *105*, 496−503.
(92) Kendrick, B.; Pack, R. T. Recombination resonances in thermal H + O_2 scattering. *Chem. Phys. Lett.* **1995**, *235*, 291−296.
(93) Troe, J. Theory of thermal unimolecular reactions at high pressures. *J. Chem. Phys.* **1981**, *75*, 226−237.
(94) Cobos, C. J.; Troe, J. Theory of thermal unimolecular reactions at high pressures. II. Analysis of experimental results. *J. Chem. Phys.* **1985**, *83*, 1010−1015.
(95) Zuo, J.-X.; Hu, X.-X.; Xie, D.-Q. Quantum Dynamics of Oxyhydrogen Complex-Forming Reactions for the HO_2 and HO_3 Systems. *Chin. J. Chem. Phys.* **2018**, *31*, 123−134.
(96) Akiya, N.; Savage, P. E. Effect of Water Density on Hydrogen Peroxide Dissociation in Supercritical Water. 2. Reaction Kinetics. *J. Phys. Chem. A* **2000**, *104*, 4441−4448.
(97) Laidler, K. J.; King, M. C. Development of transition-state theory. *J. Phys. Chem.* **1983**, *87*, 2657−2664.
(98) Glowacki, D. R.; Orr-Ewing, A. J.; Harvey, J. N. Product energy deposition of CN + alkane H abstraction reactions in gas and solution phases. *J. Chem. Phys.* **2011**, *134*, 214508.
(99) Glowacki, D. R.; Orr-Ewing, A. J.; Harvey, J. N. Non-equilibrium reaction and relaxation dynamics in a strongly interacting

DOI: 10.1021/acs.jpca.9b08789
J. Phys. Chem. A 2019, 123, 10772−10781

explicit solvent: F + CD_3CN treated with a parallel multi-state EVB model. *J. Chem. Phys.* **2015**, *143*, 044120.
(100) Kästner, J. Umbrella Sampling. *Wiley Interdiscip. Rev.: Comput. Mol. Sci.* **2011**, *1*, 932−942.
(101) Kumar, S.; Rosenberg, J. M.; Bouzida, D.; Swendsen, R. H.; Kollman, P. A. The weighted histogram analysis method for free-energy calculations on biomolecules. I. The method. *J. Comput. Chem.* **1992**, *13*, 1011−1021.
(102) Purvis, G. D.; Bartlett, R. J. A full coupled-cluster singles and doubles model: The inclusion of disconnected triples. *J. Chem. Phys.* **1982**, *76*, 1910−1918.
(103) Scuseria, G. E.; Janssen, C. L.; Schaefer, H. F. An efficient reformulation of the closed-shell coupled cluster single and double excitation (CCSD) equations. *J. Chem. Phys.* **1988**, *89*, 7382−7387.
(104) Scuseria, G. E.; Schaefer, H. F. Is coupled cluster singles and doubles (CCSD) more computationally intensive than quadratic configuration interaction (QCISD)? *J. Chem. Phys.* **1989**, *90*, 3700−3703.
(105) Dunning, T. H., Jr. Gaussian basis sets for use in correlated molecular calculations. I. The atoms boron through neon and hydrogen. *J. Chem. Phys.* **1989**, *90*, 1007−1023.
(106) Kendall, R. A.; Dunning, T. H., Jr.; Harrison, R. J. Electron affinities of the first-row atoms revisited. Systematic basis sets and wave functions. *J. Chem. Phys.* **1992**, *96*, 6796−6806.
(107) Truhlar, D. G.; Garrett, B. C.; Klippenstein, S. J. Current Status of Transition-State Theory. *J. Phys. Chem.* **1996**, *100*, 12771−12800.
(108) Frisch, M. J.; Trucks, G. W.; Schlegel, H. B.; Scuseria, G. E.; Robb, M. A.; Cheeseman, J. R.; Scalmani, G.; Barone, V.; Petersson, G. A.; Nakatsuji, H.; et al. *Gaussian 16*; Gaussian, Inc.: Wallingford, CT, USA, 2016.
(109) Gilbert, R. G.; Smith, S. C.; Jordan, M. *UNIMOL Program Suite*, available from the authors: School of Chemistry; Sydney University: NSW, Australia, 2006, 1993.
(110) Miyoshi, A. *GPOP software*, rev. 2013.07.15m7 (accessed April 10, 2019).
(111) Garrett, B. C.; Truhlar, D. G. Semiclassical tunneling calculations. *J. Phys. Chem.* **1979**, *83*, 2921−2926.
(112) Miyoshi, A. *SSUMES software*, http://akrmys.com/ssumes (accessed Sep 19th, 2019).
(113) Marcus, R. A. Unimolecular Dissociations and Free Radical Recombination Reactions. *J. Chem. Phys.* **1952**, *20*, 359−364.
(114) Matsugi, A.; Suma, K.; Miyoshi, A. Kinetics and Mechanisms of the Allyl + Allyl and Allyl + Propargyl Recombination Reactions. *J. Phys. Chem. A* **2011**, *115*, 7610−7624.
(115) Matsugi, A. Collision Frequency for Energy Transfer in Unimolecular Reactions. *J. Phys. Chem. A* **2018**, *122*, 1972−1985.
(116) Troe, J. Theory of thermal unimolecular reactions at low pressures. II. Strong collision rate constants. Applications. *J. Chem. Phys.* **1977**, *66*, 4758−4775.
(117) Brooks, B. R.; Bruccoleri, R. E.; Olafson, B. D.; States, D. J.; Swaminathan, S.; Karplus, M. CHARMM - a program for macromolecular energy, minimization, and dynamics calculations. *J. Comput. Chem.* **1983**, *4*, 187−217.
(118) Brooks, B. R.; Brooks, C. L.; Mackerell, A. D.; Nilsson, L.; Petrella, R. J.; Roux, B.; Won, Y.; Archontis, G.; Bartels, C.; Boresch, S.; et al. CHARMM: The biomolecular simulation program. *J. Comput. Chem.* **2009**, *30*, 1545−1614.
(119) Vanommeslaeghe, K.; Hatcher, E.; Acharya, C.; Kundu, S.; Zhong, S.; Shim, J.; Darian, E.; Guvench, O.; Lopes, P.; Vorobyov, I.; et al. CHARMM General Force Field: A Force Field for Drug-Like Molecules Compatible with the CHARMM All-Atom Additive Biological Force Fields. *J. Comput. Chem.* **2010**, *31*, 671−690.
(120) Kuchitsu, K. *Structure of Free Polyatomic Molecules-Basic Data*; Springer: Berlin, 1998.
(121) Aimoli, C. G.; Maginn, E. J.; Abreu, C. R. A. Force field comparison and thermodynamic property calculation of supercritical CO_2 and CH_4 using molecular dynamics simulations. *Fluid Phase Equilib.* **2014**, *368*, 80−90.
(122) Potoff, J. J.; Siepmann, J. I. Vapor-liquid equilibria of mixtures containing alkanes, carbon dioxide, and nitrogen. *AIChE J.* **2001**, *47*, 1676−1682.
(123) Nosé, S. A unified formulation of the constant temperature molecular dynamics methods. *J. Chem. Phys.* **1984**, *81*, 511−519.
(124) Hoover, W. G. Canonical dynamics: Equilibrium phase-space distributions. *Phys. Rev. A* **1985**, *31*, 1695−1697.
(125) Darden, T.; York, D.; Pedersen, L. Particle mesh Ewald: An N log(N) method for Ewald sums in large systems. *J. Chem. Phys.* **1993**, *98*, 10089−10092.
(126) Essmann, U.; Perera, L.; Berkowitz, M. L.; Darden, T.; Lee, H.; Pedersen, L. G. A smooth particle mesh Ewald method. *J. Chem. Phys.* **1995**, *103*, 8577−8593.

DOI: 10.1021/acs.jpca.9b08789
J. Phys. Chem. A 2019, 123, 10772−10781